Book of Tutorials and Abstracts

European Microbeam Analysis Society

EMAS 2019

16th

EUROPEAN WORKSHOP

on

MODERN DEVELOPMENTS AND APPLICATIONS IN MICROBEAM ANALYSIS

19 to 23 May 2019
at the
NTNU, Realfagbygget
Trondheim, Norway

Organised in collaboration with:
Norwegian University of Science and Technology
(NTNU)

A DEEPER INSIGHT INTO MATERIALS: POTENTIALS AND LIMITATIONS OF μ-XRF

Roald A. Tagle Berdan, F. Reinhardt, U. Waldschläger, T. Hill and T. Wolff

Bruker Nano GmbH
Am Studio 2D, 12489 Berlin, Germany
e-mail: roald.tagle@bruker.com

In 1998 Roald Tagle received a Diplom (German equivalent of MSc) in Chemistry at the Universität Leipzig. In 2004 he obtained a PhD from the Department of Mineralogy - Museum of Natural History in Berlin and the GeoForschungsZentrum (GFZ) Potsdam, for his work on the development of a method for the identification of projectile components in impact crater materials. Between 2005 and 2007 he held a postdoc grant from the „Deutsche Akademie der Naturforscher LEOPOLDINA". He was a visiting scientist at the Department of Geology of the Vrije Universiteit Brussels, and the Department of Planetary and Space Sciences of the University of New Brunswick, Canada. In 2007 he joined Bruker Nano GmbH (Berlin, Germany), where he is currently working on μ-X-ray instrument research and development.

1. ABSTRACT

Micro-X-ray fluorescence or X-ray fluorescence microanalysis, as it was called at the beginning is a spatially resolved version of X-ray fluorescence analysis. This analytical technique was first described more than 50 years ago [1-7]. Since then, it has remained mostly a niche technique, quite common in several industrial application fields, e.g., coating analysis, but without becoming part of standard analytical techniques presented and used in universities and other higher education facilities, even though early publications highlighted the same principle advantages that we see today. These advantages include: The possibility of non-destructive sample analysis, the possibility to study well defined small sample areas or non-homogenous materials. In addition, the technique is fast with major and trace element sensitivity. In recent years, a series of technological developments, from excitation sources, to enhanced detection possibilities and signal processing capabilities and algorithms have allowed improvement in the performance of the technique, making it useful as a standard analytical tool. The aim of this presentation is to give a hint of what is possible and where the technique is now in terms of analytical performance.

2. INTRODUCTION

Among the most universal and best-known techniques for material analysis are optical and electron microscopy or electron probe microanalysis (EPMA), X-ray diffractometry (XRD), X-ray fluorescence (XRF), as well as IR and Raman. These techniques combine the possibility to magnify, visualise compositional variations, characterise crystallographic properties and determine major and trace element composition of a variety of samples. μ-XRF is relatively universal, and from an application point of view, it shows multiple overlaps when compared with these techniques. It provides significant complementary information in the analytical process of complex sample evaluation.

Sample preparation is usually complicated and time-consuming and there is a natural tendency to "optimise" the number of samples studied, which increases the chance of analytical misinterpretation due to non-representative sampling. Analytical techniques that could work with only minimal sample preparation are therefore certain to support and help to optimise the number of samples processed. Such analytical techniques have developed significantly in recent years. Technological advances in the fields of miniaturisation and computational power lead to the development of even handheld spectroscopic instruments which, utilising IR, Raman, or even X-ray fluorescence (XRF), permit measurement of samples directly and with no preparation at all. A good material characterisation, in addition to detailed composition can be obtained within seconds or minutes. Most of these instruments particularly XRF-based instruments originated in the field of metal sorting as simple devices and have developed to sophisticated instruments reaching a more academic, research and development environment in recent years. Here, we would like to focus on XRF as a "first-line technique," not in its simpler hand-held version, but on the more sophisticated technique of tabletop μ-XRF.

We will discuss possibilities and limitations of μ-XRF often by comparing to electron excitation fluorescence spectroscopy as a reference technique. Electron beam-based fluorescence analyses (SEM, EPMA) and μ-XRF show certain similarities, in principle, but also major differences. It is these differences, which offer the largest analytical potential. Possibilities and limitations will be discussed using examples covering evaluation of quantitative and qualitative samples highlighting the possibility to obtain superficial compositional information and information from below the sample surface itself.

3. WHAT IS μ-XRF?

The obvious difference between conventional X-ray fluorescence analysis and μ-XRF is that μ-XRF uses a small spot to excite a predefined sample location. In conventional XRF, large sample areas of several millimetres are usually analysed with the purpose of quantification. Therefore, in conventional XRF samples are prepared to optimise the conditions for quantification. This preparation involves homogenisation often in combination with a reduction of the matrix effects by diluting the samples with low density materials. The sample preparation procedure ensures a standardized sample evaluation routine and high reproducibility of results. However, inhomogeneity of the sample can be an important aspect of the analytical question and most sample preparation is inherently destructive. Here is where spatially-resolved XRF, can play a key role. μ-XRF as a technique is designed for inhomogeneous samples. Quantification is still feasible but requires more caution and evaluation by the user.

3.1. The beam

Use of a small defined beam, similar in principle to an electron beam but larger, allows studies of the compositional variations of inhomogeneous samples. The small X-ray beam can be produced by using collimators or reflective optics such as mono- or polycapillary lenses. The main disadvantage of collimators is that the intensity decreases proportional to the collimator area, and for spot sizes below 500 μm diameter the beam intensities reaching the sample are extremely low. Therefore, applications for which larger beam diameters are needed typically use collimators. For smaller beams, mono- or polycapillary lenses using the principle of total reflection are used. These lenses "collect" the X-ray close to the anode and "guide" them to small spot on the sample surface. Polycapillary lenses are much more efficient in the transport of X-rays than monocapillary lenses but monocapillaries are by far simpler to produce. Polycapillary lenses have evolved to be the state-of-the-art option when a combination of brilliance and small spot are required in a benchtop instrument.

From an application point of view, lenses have two main limitations to consider when discussing spot size. First, the smaller the spot size, the lower the final intensity of the beam on the sample and second, a smaller beam size also implies a small working distance. Polycapillary lenses are currently a good compromise between intensity, spot size and working distance, yielding a

15 µm to 25 µm spot size with a working distance of approximately 8 mm. For applications requiring smaller spot sizes, a compromise between both parameters would be needed. In addition, the "transmission" efficiency of a lens depends on the critical angle for external total reflection and therefore on the energy/wavelength of the X-rays. For lower energies, the acceptance angle is bigger than for higher energies which results in a significant loss of efficiency in the high energy range. Lower energies on the other hand are more likely to be absorbed by the glass of the capillaries. Therefore, the transmission of a polycapillary lens is much higher in the mid energies than it is below 4 keV and above 20 keV. This effect does not apply to collimators. Here loss due to spot size is the same for all energies.

The small beam and localised measurement position can be used in single point mode or in scanning mode. In the latter, ideally, the full spectrum is saved for each measured location. This position tagged spectroscopy then allows not only for creating element distribution maps but also for the complex post-processing procedures which a rather common on today SEM-EDS analyses.

In an SEM it is rather easy (and very fast) to deflect the focused electron beam in order to "scan" over the sample. In µ-XRF the movement of excitation relative to the sample calls for mechanical movement of either the excitation unit or the sample itself. For closed instruments moving the sample is the common approach, open beam instruments usually move the excitation unit. Exceptions here are synchrotron radiation facilities, where, even when the setup is open beam, moving the source is not an option.

3.2. The X-ray source

µ-XRF instruments can be equipped with various types of X-ray sources and anode materials. Of all possible target options, rhodium is the most universal. This, on the one hand side, is due to its high melting point and good thermal conductivity, on the other hand, the Compton-scattered characteristic lines of rhodium overlap only with the elements Ru, Tc, Pd, and Cl. The overlap with Cl can be eliminated by using appropriate primary filters. Note that this is also possible for K-lines but significantly more complex. For special applications where high sensitivity for the element Cl is needed, it is possible to select other anodes such as Ag [12], trading this advantage for a partial overlap with potassium for the Ag-L lines and Rh, Pd, Cd, In and Sn in the high-energy region. Excitation efficiency for element lines whose fluorescence lines are above the characteristic lines of the anode material e.g., Rh or Ag, is limited. The low transmission efficiency of polycapillary lenses for high energy radiation adds to this effect. The use of a collimator as a simple optic can help to somewhat improve the excitation of high-energy lines, but again, the trade-off will be generally lower intensity when small spots are considered. Tungsten can also be used as anode material. The high-Z material has a higher bremsstrahlung yield and with this anode and a collimator optic, it is possible to lower the detection limit of the elements from Cd to Te even down to the low parts per million range.

3.3. The filters

Primary filters are a common tool in µ-XRF where they are used to change the excitation spectrum or adapt it to the analytical task. Filters are made of one or more metal foils of known thickness. Several things should be considered in case of using a filter. 1) The filter material should not produce a signal that can be scattered from the sample and hinder detection of elements in the sample by overlap, 2) Filters should not create a strong absorption edge feature in the spectra because it hampers good background determination, and 3) Filters reduce the excitation efficiently of low energy lines compared to an unfiltered measurement. However, after all these effects are carefully considered filters are very helpful to eliminate specific energy ranges of the excitation spectrum. This is chiefly eliminating the characteristic lines of the anode to reduce overlap with lines from the sample, e.g., Rh-L lines, W-L lines, or even Rh-K lines in some instances. Primary filters also reduce the bremsstrahlung component resulting in a better peak-to-background ratio and can also reduce certain energy ranges of the spectrum that would be diffracted to produce artefact peaks on a sample of crystalline nature.

3.4. The detectors

Fast analysis requires not only high excitation intensity but also detectors with high signal throughput, which collect lots of counts and transfer them into the spectrum. There are several ways of increasing the detected signal: The biggest effect is the solid angle of detection, which can be increased by either large active detector areas or by getting the detector very close to the sample. Another possibility is to use multiple detectors. Multiple detectors allow processing signals in parallel and enable the user to "look" at samples from different directions. For the interpretation of element distribution images, the detector has to be considered to be the light source "illuminating" the sample and the beam (electron or X-ray) as the eye that is looking at the sample. This allows an easy understanding of the "shadow" regions on samples with topography. By using multiple, or even coaxial detectors, the shadow-effect is minimised (Fig. 1).

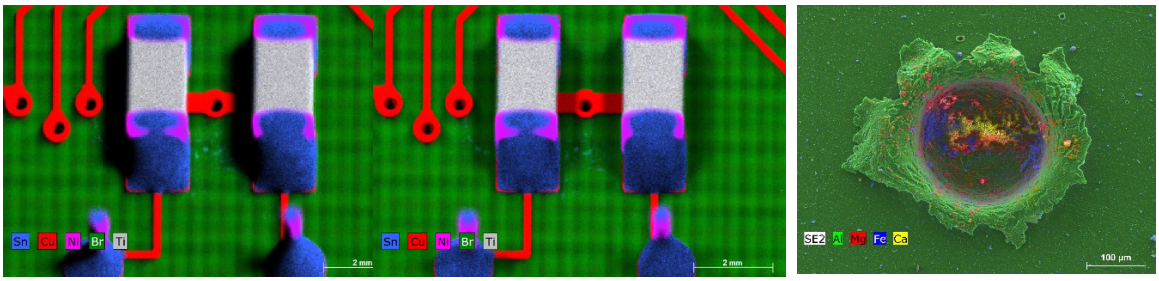

Figure 1. Three element distribution maps. Element distributions were measured with one detector (left), note the "shadow" to the left side of the electronic component; the second image (middle) was acquired with two detectors, note only partial shadow right and left; the last image from an SEM (right) was acquired with an annular coaxial "Quad" detector, note the lack of "shadow" on this element distribution image.

The lowest detectable element is not defined by excitation efficiency or absorption effects between sample and detector. The decisive factor is the transmittance of the entrance window of the detector. In µ-XRF the common type of detector windows is made of beryllium. They are usually 8 µm or 12.5 µm thick, depending on the detector size. A beryllium window limits the lowest detectable element to sodium as the window effectively absorbs energies below 1 keV. Light-element windows like those available in SEM-EDS shift the limit of visible elements down to carbon. Figure 2 shows a µ-XRF element map of a fresh strawberry. This measurement ran overnight under He atmosphere (to prevent vacuum drying of the sample) with light element detectors.

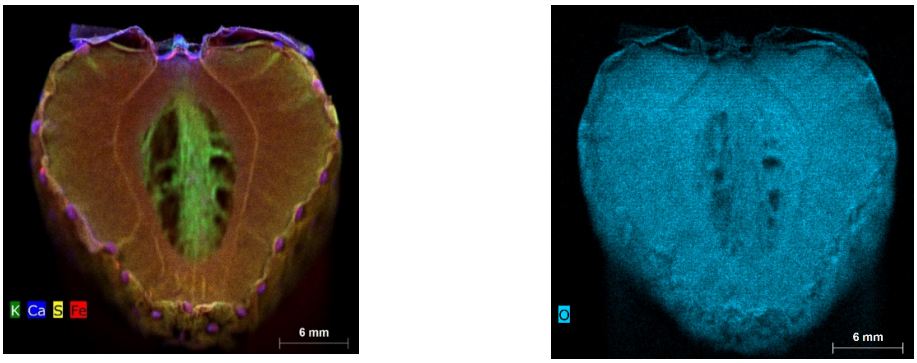

Figure 2. Element distribution in a fresh cut strawberry. The measurement was performed in helium atmosphere to measure light elements such as oxygen in a wet sample.

In the lower energy regime, overlap between fluorescence lines is a more pronounced problem than in the high-energy range. This in combination with the drastically reduced information depth calls for careful interpretation of the results. The same is true for quantification results using fundamental parameters (FP) quantification. Using X-ray excitation of, e.g., 50 keV for the excitation of a light-element sample will cause light elements to not only to be excited directly by the X-rays but also by photo-electrons. This secondary excitation source is not considered in common FP quantification models.

3.5. The sample

X-ray fluorescence analysis is a non-destructive technique and the sample can be analysed without prior sample preparation. This makes the µ-XRF instrument extremely accessible for fast initial assessment of samples by simply placing the sample in the chamber and analysing. However, this approach does not always yield optimal results. To obtain the very best data by performing an optimal analysis, it is important to consider that sample preparation can greatly influence the results obtained from a measurement.

3.5.1. Sample preparation. The ideal sample for an electron-based excitation should be conductive. For µ-XRF analysis this is not required. In principle, any sample can be measured directly and without any sample preparation, including liquids, solids or powders. However, some preparation or use of a specific sample holder might be required to achieve the best results. A measurement of the major and minor elements requires very little preparation and should always be possible. Only an intricate geometry might pose a problem in this case. For ideal quantitative analysis, the sample should be placed horizontal to the measurement plane, it should be infinitely thick (see later discussion), and homogenous within the analysed volume. Note that the analysed volume depends on the sample and elements and may be in the cubic micrometre- or millimetre-range or in some cases even more. Any deviation from this ideal sample tends to complicate the task or can make a quantification even impossible. Besides preparation on the sample itself, the manner in which you place the sample in the chamber is crucial in µ-XRF due to the high information volume. Aluminium holders such as those used in SEM analysis are not at all useful for small and light samples in µ XRF as the trace elements in the aluminium holder (especially Pb and Bi) can be excited along with elements from the sample, contaminating the spectrum and giving incorrect compositional information. For thin samples such as paper, parchment, foil, leaves or cloth it is recommended to measure the sample elevated over a polymer support to reduce the scattering from the material below the object. In µ-XRF as the analysed volume is important, the 3rd dimension should always be kept in mind.

For very light elements (from C to Cl) the air gap between the sample and the detector acts as an efficient absorber. Sodium fluorescence is absorbed by 99 % under ambient conditions. This effect decreases with higher energy. Absorption by air for Ca, for example, is below 20 % (see Table 1).

Table 1. Calculated transmission for different element lines at different air pressures as well as for He atmosphere. Values calculated using https://xrfcheck.bruker.com/FilterTransmissions.

Element	Energy in keV	Air 1000 mbar	Air 200 mbar	Air 20 mbar	Air 2 mbar	He 800 mbar
C	0.3	0.0	11	80	98	43
N	0.4	0.4	33	90	99	71
O	0.5	0.0	0	54	95	87
F	0.7	0.0	1	65	96	94
Na	1.0	0.1	23	86	99	98
Ca	3.7	80	96	100	100	100
Fe	6.4	96	99	100	100	100

calculated for 20 mm distance betwenn sample and detector
Air = 78.115 % N2; 20.95 % O2; 0.934 % Ar

To overcome the absorbance problem many µ-XRF instruments are equipped with vacuum pumps to decrease this effect. Beryllium windows limit the lowest detectable element to Na and it is usually sufficient to create a pressure of 20 mbar, which allows the transmission for Na-K to increase from less than 1 % to almost 90 %. When aiming to detect very light elements a

vacuum lower than 20 mbar is required. Another option is to exchange the air with helium. The exchange of air with He allows measurements of samples for light elements without exposing them to a low-pressure environment and for most elements this even comes without significantly compromising the sensitivity.

3.5.2. Interaction with the sample. With the highly focussed beam, small areas of the sample can be exposed to relatively high photon fluxes, even if only low power X-ray tubes are used (< 50 W). An estimation of the deposited energy per area based on our FP quantification software, FPQ [21] provides values in the order of 25 W/m². However, the energy deposited per area is only a tiny fraction of that of electron excitation (10 MW/m² in a spot of 1 µm for 15 kV, 5 nA), and, therefore, sample damage is marginal in comparison. Changes such as temperature increases are less likely to occur in the case of benchtop µ-XRF instruments. Among sample changes known so far and described for µ-XRF is the formation of metastable colour centres, e.g., in glasses or enamel. Such defects tend to "regenerate" after a certain time (e.g., [19]). Other studies of possible effects are currently ongoing at several institutions; therefore, more is expected in the years to come.

3.6. Spatial resolution

Both electron and photon excitation use an energy-dispersive X-ray detection system. Therefore, the two methods appear to be very similar. One of the main differences is spatial resolution. In electron excitation, the electron beam can be focussed down to a few nanometres and the interaction volume can be efficiently "adapted" to the application by adjusting the electron acceleration voltage. In the case of photons, the focussing options are limited and smaller beams tend to compromise the intensity and the working distance. Additionally, options of controlling the penetration depth and therefore the interaction volume of photons in the samples are also limited. In XRF, both excitation and detection are based on photons. As excitation always has a higher energy than emission, emission is the limiting process in terms of information volume. This is contrary to electron excitation, where the mean free path of the electrons within the sample – the penetration depth – is always lower than that of the photons and is, hence, the limiting factor. In XRF the information depth is the value to be considered. It is the depth from which a defined amount of the fluorescence X-rays produced in the sample can still reach the detector. Definitions of information depth usually vary between 90 % and 1/e (~ 37 %) of produced fluorescence in the sample.

Information depth depends on the average atomic number of the sample and the fluorescence energy of the element in question. Excitation of an element's fluorescence line is most efficient directly above the respective absorption edge. Higher energy photons can excite the atom, but the efficiency quickly diminishes. Thus, the information depth can be reduced by changing the acceleration voltage within the X-ray tube (and thereby reducing the amounts of high-energy photons in the excitation spectrum), but the effects are marginal compared to the effect in electron excitation. Therefore, the most effective possibility to reduce information depth is to

evaluate a lower-energy fluorescence line of the same element. For example, using Pb-M instead of Pb-L reduces information depth from ~10 μm to approximately 1 μm in an Fe matrix. In an oil painting, which usually is a much less dense material than Fe, the effect is significantly more pronounced (Fig. 3).

Figure 3. These element distribution images shown the distribution of lead in a painting. The first image shows the Pb-M lines at 2.4 keV and the second the Pb-Lα line at 10.54 keV. The difference in energies allows "display" of the element distribution at different depths. The L-lines show the painting down to the grounding, including the damaged areas on the left side, and the M-lines show the topmost thin layers of Pb pigments present at the painting's surface.

The high information depth requires consideration of the question of 'infinite thickness' in a wide variety of samples. Infinite thickness usually is a prerequisite for bulk quantification models. If the thickness of a sample could be increased continuously, the "infinite thickness" is the specific sample thickness from which on the fluorescence signal coming from the excited sample for any given element does not increase anymore (usually neglecting secondary excitation by fluorescence or scattered high-energy photons). As can be seen in Fig. 4, an infinite thickness may reach the centimetre-range when analysing heavy elements in light matrix (RoHS screening or similar).

3.7. Excitation efficiency

The ionisation cross-section for most elements is higher for photons than for electrons. As a rule of thumb, it can be said that for lines above Ca-K, electron excitation is less efficient than photon excitation. In addition, for an effective photon excitation, no overvoltage ratios have to be considered. Any photon with an energy above an element's absorption edge can excite the element. For example, with a 50 keV X-ray tube the K-edge of europium (Z = 63, K-edge at 48.5 keV) can be excited.

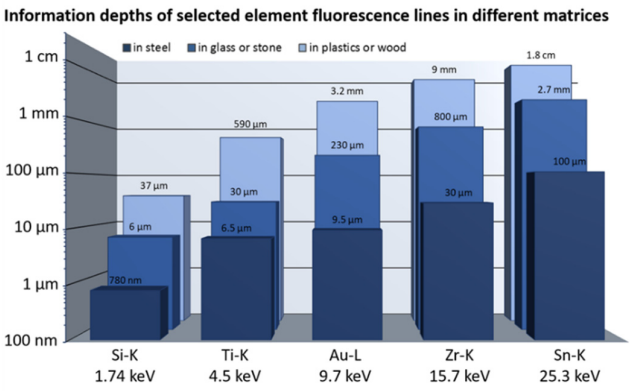

Figure 4. Information depth calculated for different material and different element lines for a standard M4 Tornado and a remaining intensity of 90 % was used as criteria. Calculation performed using FP software developed by Bruker https://xrfcheck.bruker.com/.

3.8. Detection limits

The differently effective excitation and the much higher volume of analysis lead to very different detection limits when comparing electron- and photon-based excitation.

The figures above aim to illustrate the differences in the detection limits. Detections limits are extremely dependent on sample types and cannot be stated for the technique in general. The detections limits for Cu in a glass are at least one order of magnitude lower than in an Fe sample. Detection limits also depend on the presence or absence of adjacent element lines. This is valid both from a spectral point of view where line overlap may pose a problem, and also from a physics perspective as energetically close absorption edges may have a very pronounced effect on information depth, and therewith on the number of probed atoms. However, the general trend in Fig. 5 remains valid. The increase of one order of magnitude around Z = 40 is a result of shifting from K-line to L-line quantification above the Rh-K line.

4. APPLICATION EXAMPLES

4.1. Quantification

Just as in electron-based EDX, µ-XRF is an analytical technique with multiple quantitative options. Quantitative XRF analysis can be done based on empirical models (standard-based) or based on fundamental parameters (FP). A well-known full empirical model is the Lucas-Tooth approach. It is based on measured intensities and the concentration of a given element depends on the intensity of its characteristic line and the intensity of the other elements in the sample. The quality of standard-based quantification is limited by the quality of available standards and the similarity of the sample to those available standards. For a calibration using Lucas-Tooth, a relatively large set of samples is required, and the calibration will be valid only for the concentration range defined by the standards.

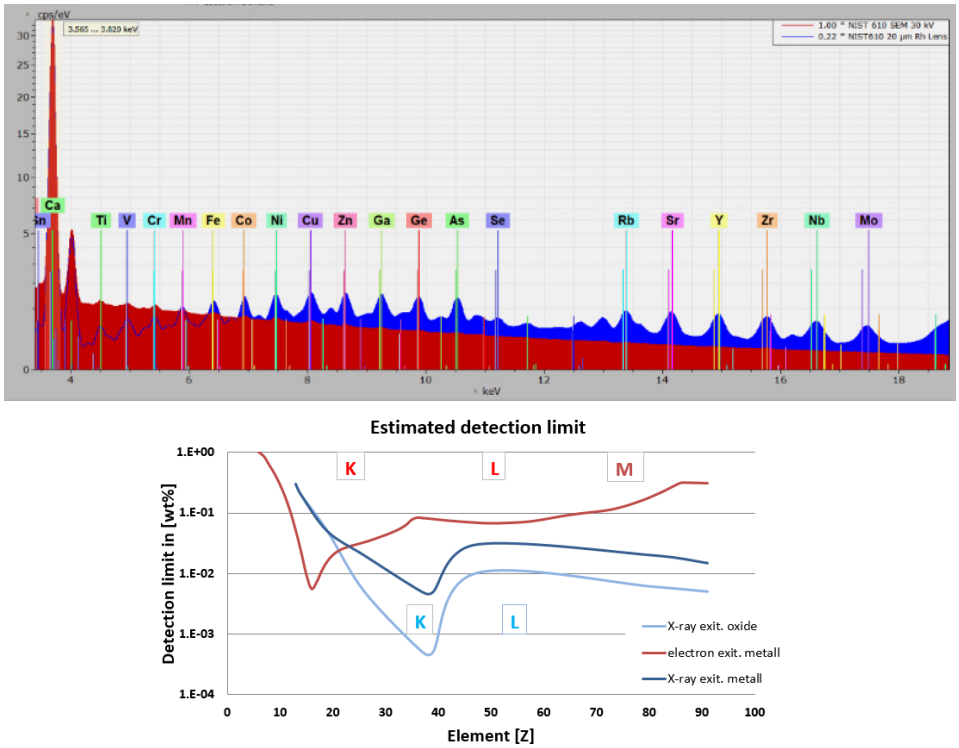

Figure 5. The top figure shows two spectra from a NIST 610 glass. The spectrum in blue was taken with a µ-XRF system using Rh tube at 50 kV and 600 µA, the red spectrum was taken in an SEM using 30 kV.

In contrast to conventional XRF where samples and sample preparation can be rather standardised (e.g., metals, concrete), the fields of application of µ-XRF go into more complex material analysis where standards or reference samples might not even be available in high enough quality. Therefore, µ-XRF strongly requires the flexibility of an FP quantification. In general, bulk FP models are applicable to infinitely thick, homogeneous samples, which is to a certain extent inconsistent, as µ-XRF is an analytical technique designed for inhomogeneous samples (e.g., [11]). This means that for quantification, a homogeneous area must be identified within the spatial resolution of the X-ray beam and the information depth of the analysed elements.

4.1.1. Fundamental parameters applied to steel samples. The fundamental parameter model rests on a fully mathematical description of the fluorescence based on sample composition, natural constants (the fundamental parameters) and some instrument-specific parameters. The FP quantification used here is based on the Sherman equation [13]. The approach includes an iterative process of solving the Sherman equation, where the measured spectrum is compared to a spectrum calculated for the sample. The composition of the sample used for calculation is varied in an iterative process until the measured and the calculated spectrum match each other.

Despite there being a significant improvement of performance in recent years, FP is still considered sometimes as "semi-quantitative" and to be less accurate than standard-based quantification. However, the high precision of standard-based quantification is limited by the quality of reference samples existing, which are in fact not always the best. Unfortunately, there are currently very few existing certified reference samples for small spot analysis. Depending on the alloy type, metals may suffer from varying degrees of micro-segregation, e.g., Cu-Pb alloys, causing inhomogeneity. Mineral samples are often not as homogeneous as expected due to zoning or other properties, and powder samples are usually ground down to < 60 µm, which implies that within the probing volume grains are analysed individually. Of all these materials, glass is the most user-friendly in terms of homogenisation. Nonetheless, even though issues such as inhomogeneity exist, the existing reference samples can be used, but with caution.

Figure 6 depicts results obtained from a set of 15 certified reference stainless steel samples from ARMI evaluated by µ-XRF and quantified using FP. They were measured using an M4 Tornado with a polycapillary lens, and a Rh tube operated at 50 kV and 200 µA. Each sample was measured at 10 points with 10 s live time per point and at 20 mbar pressure. Quantification was performed using the FP algorithm delivered standard with the instrument. Steels are rather homogeneous heavy matrix samples with a limited information depth for the included element and typically possess flat surfaces. It is, thus, easy to fulfil the criteria for the applicability of FP quantification.

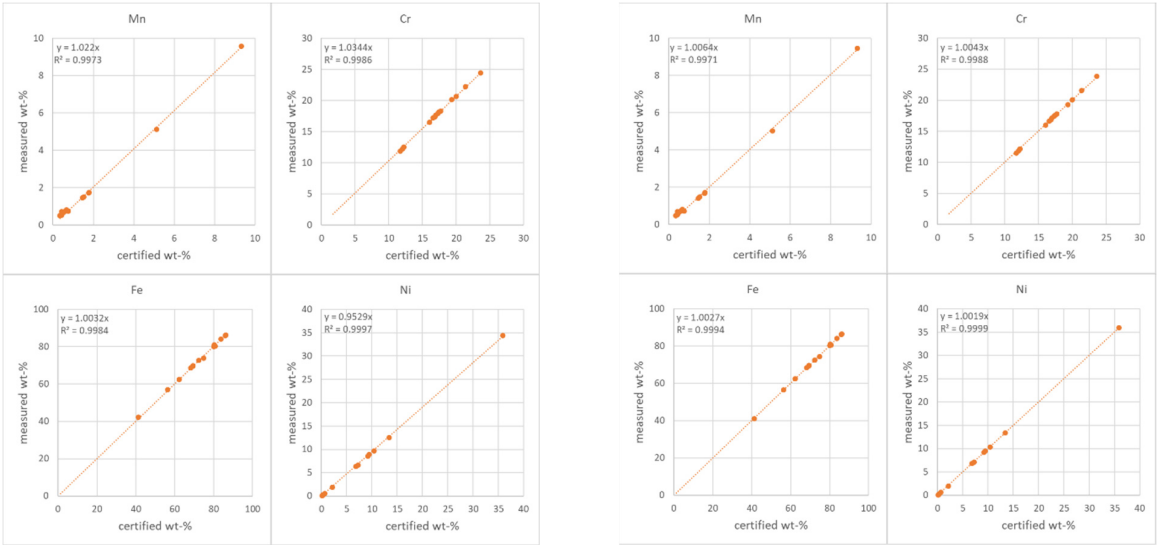

Figure 6. The left side shows 4 plots with correlations of the FP-quantified results for the steel samples versus their reference values. The slope is used to create a type calibration factor. This factor is applied to the quantification. Results after the correction are shown in the 4 plots on the right side. Here a significant improvement can be observed, i.e., the slopes of the correlations is 1 within 3 permille.

The fundamental parameters for the K-lines of metals are well known. Thus, the mathematical model for the quantification based on the Sherman equation [13] yields very good results, as demonstrated in Fig. 6. The linear relation between known compositions and quantified concentrations for the elements is particularly striking. For some elements, especially Cr and Ni, the correlation is linear, but the slope of the correlation function is not as close to 1 as for the other elements. This is due to the fact that, in the case of stainless steels, a tertiary process is prominent which is usually not included in the calculations. Ni fluorescence is effectively absorbed by Fe in order to produce secondary Fe photons, which in turn are absorbed by Cr to produce tertiary Cr photons. This tertiary process is not included in the mathematical model and, hence, Ni concentrations are usually underestimated (by 3 - 5 %) and Cr concentrations are overestimated by a similar margin. Still, there is a linear correlation between given values and measured values. This tertiary effect is easily accounted for by calibrating. As this calibration (i.e., virtually changing the assumed sensitivity of the instrument for the respective elements) is valid only for stainless steels (where Cr, Fe, and Ni are abundant in significant concentrations) it should be called a "type calibration" and, if used on other sample systems (even other metal alloys), will make results worse. For stainless steels it can yield optimal quantification results.

A second challenge with steel samples is the prominence of diffraction peaks. They can be highest in the energy regions where the primary radiation is most intense. The highest contributions of the bremsstrahlung background of the tube transmitted through the polycapillary optic are in the energy region of the 3d-metals' K-lines. This, together with the (multi-)crystalline nature of steels yields a multitude of diffraction peaks in the energy region of interest. This can pose a problem especially for the quantification of minor elements (e.g., V, Mn, Co). In Fig. 7 the quantified values for vanadium are shown plotted against the certified concentrations. On the left side, the values are shown as measured without a filter. The correlation seems to be split up into two populations.

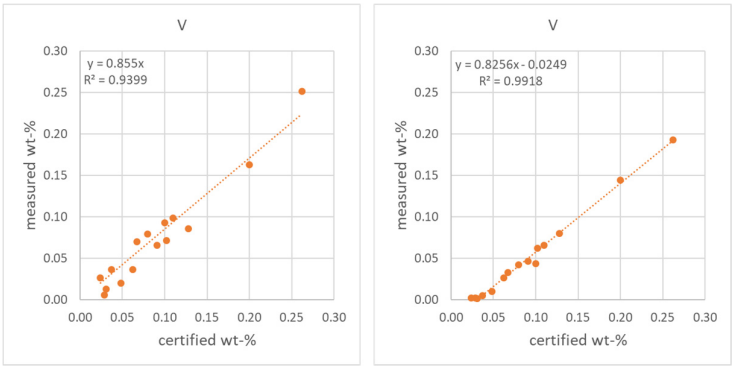

Figure 7. Vanadium FP-quantified results versus reference values, measurements without a primary filter (left) and with a primary filter (right). Note that the results for the filtered measurements shows a better correlation, but that the correlation has an offset on the x-axis.

A closer look at the spectra subsequently shows a diffraction structure in the region of interest of the V-K lines, which in this case increases the quantification results by ~ 0.3 wt%. Changes in the quantified values of this magnitude are relevant for minor elements quantification. One

solution to ameliorate this effect is to measure the same positions with a primary beam filter. The quantification results then fall into one line – the lower of the two populations (right panel). This line, just like those of the main elements, shows a linear correlation which can be corrected to a slope of 1 by applying a type calibration. Another striking feature of the shown correlation is that it does not run through the point of origin. All vanadium concentrations certified to be below ~ 0.3 wt% are quantified to 0 wt%. This gives a good indication of the detection limits of vanadium in stainless steels.

Effects like this offset can also hint at systematic errors. In this case, the fundamental parameters that designate the atomic Kβ/Kα fluorescence line ratios are of vital significance for accurate quantification of low amounts of the metals.

While most FPs are impossible to assess with laboratory equipment and need to be determined at large facilities like synchrotron radiation sources, other FPs are seemingly addressable with laboratory equipment and table top instrumentation. This is especially true for the fluorescence line ratios of pure elements, especially in energy-dispersive spectroscopy where most of the sub-lines cannot be resolved anyway.

There is a multitude of publications for FPs in general and (K) fluorescence line ratios in particular [13-15]. Among these publications, the database of Elam [16] stands out for its holistic character and is, hence, often used for FP-based XRF quantification, also by Bruker. The values therein are extracted from other papers and missing values are extra- or interpolated based on polynomials.

Given the number of theoretical and experimental publications on the topic it is surprising how much the database values which are currently used differ from each other. For Fe for example the Kβ/Kα ratio can be found between 0.135 [14] to 0.143 [16] which accounts for 6 % relative deviation.

Even for common materials such as 3d-transition metals, the K-line intensity ratios, which are only defined by transition probabilities and absorption effects, show a surprising lack of accuracy even given that the preparation of pure element samples is simple and the line energies are in a range where the EDS quantum efficiency is well known. This affects the quantification of 3d-transition metals as the Kβ-line shows a large overlap with the Kα-line of the successive element, e.g., Ti-Kβ and V-Kα (Fig. 8).

In order to improve the quality of our FP based quantification, different approaches towards assessing the correct values for the line ratios were evaluated. Several X-ray analytical methods and numerical approaches were employed: Straightforward energy-dispersive EPMA and total reflection ED-XRF (TXRF) measurements were carried out, both of which possess only minimal or negligible self-absorption effects in the detection channel and should, hence, represent the correct line ratio. Complementarily, micro-ED-XRF measurements were carried out with

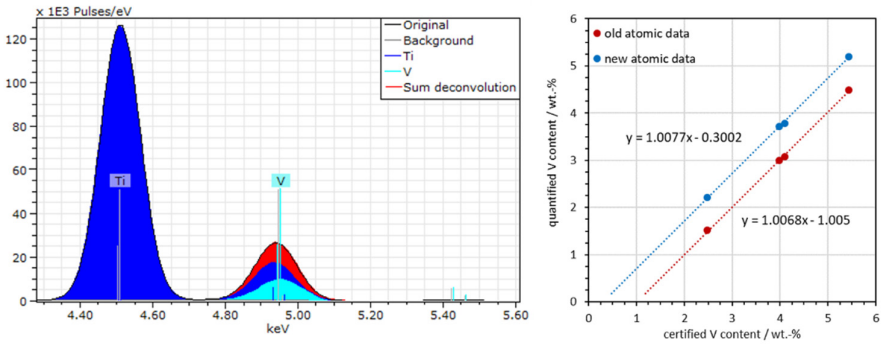

Figure 8. Left) fit of Ti and V K-lines depicting the overlap and importance of correct Kβ/Kα line ratios. Right) quantification employing common database values [16] and new ratios. With the reassessed line ratio the lower quantification limit of V is improved from 1 wt% to 0.3 wt%.

different primary beam filters. In this way, the effective depth for the production of X-rays was varied and self-absorption led to XRF spectra with different Kβ/Kα line ratios. The line intensities in the different EDS spectra were determined by peak fitting with different background models. These intensities in turn were used as input parameters for a fit, which employed an FP-based full-forward spectrum modelling and used the atomic line ratio as fit parameter.

The calculated atomic line ratios yielded improved Kβ/Kα line ratios. The benefit of this is best shown on the example of Ti-V-alloys. If the Ti-Kβ is too high with respect to the Kα, less V is needed to fill the summed joint peak around 4.95 keV. With a correct Ti-Kβ line intensity, more V will be calculated. This improves the methodological quantification limit from 1 wt% to 0.3 wt% of V in Ti-V-alloys.

In summary, FP offers the possibility to not only quantify many different samples, but to also use a simple one-point calibration to correct for minor deviations due to still-existing simplification in the FP model used([e.g., [9-10]). The FP parameters are by far not all known with the best possible precision, therefore more work is needed to continue improving the performance of FP calculation in the future.

4.1.2. Empirical quantification.

4.1.2.1. Trace element sensitivity. One of the main advantages of µ-XRF is its trace element sensitivity. Many applications require more than just deriving major element composition. Often the trace elements are those that provide a crucial piece of the story. The example presented here combines several topics: One is the use of ideally homogenous, pressed nanopowder samples made from certified reference materials. Second is the possibility to determine elements with concentrations down to the low ppm-level. In addition, pitfalls that arise from differing levels of knowledge of the "real composition" of a reference sample are discussed.

Powdered certified reference materials (CRM) made from minerals and rocks are often not suitable as reference samples for microbeam techniques, as the question of a true representative sampling is always one of the main issues to consider. The samples presented here were prepared by using a sophisticated milling protocol, which ensures that most of the particles are < 200 nm. After milling, the powdered samples are pressed. The small grain size and the applied pressure causes the material to "solidify" to a hard, flat, stable sample with glass-like quality. A comparative study of a set of 10 different CRM samples was undertaken to validate the performance of the sample preparation. For each reference material, a pressed reference sample of the original powder was prepared, as well as three nanopowders of the same sample for comparison.

The samples were scanned using a μ-XRF instrument. The element images were obtained using a region of interest (ROI) approach where the intensity of a pre-defined region around the element line is displayed after scaling it to an intensity level of 255. As can be seen from the elemental distribution analysis in Fig. 9, homogeneity increased in the sample from top (original powder) to the three nanosamples. This was valid for the complete set of 10 samples.

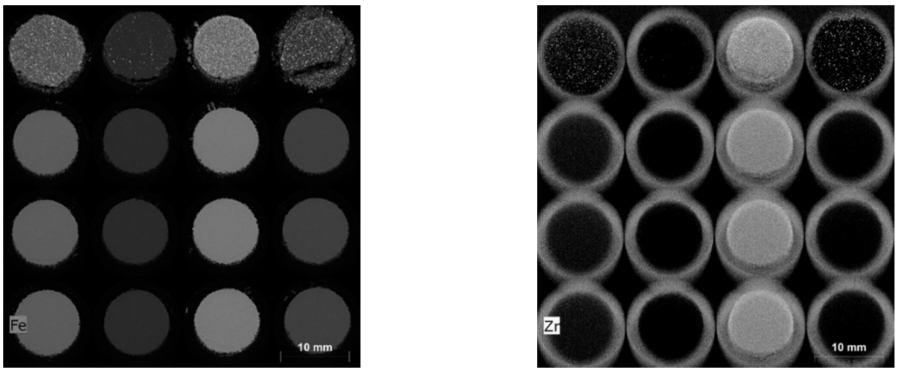

Figure 9. Element distribution image of 4 different CRMs. Top row is original CRM powders; the three rows below are the same powder after milling to the nanograin size.

In addition to the gain in homogeneity, most nanopowered samples showed a relative depletion in the Al-intensity when compared to the respective original sample material. For other light elements such as Mg, the effect was not observed. The reduction of the Al-intensity correlates with the amount of iron in the sample. To be noted: Iron is the heaviest main component among the samples. The explanation for this observation comes back to information depth issues discussed previously.

In natural mineral samples, mafic mineral components (Fe-rich minerals, e.g., olivine) are usually not rich in Al, which is mostly associated with felsic minerals such as feldspars. As illustrated in the schematic drawing (Fig. 10), the grain size in powdered CRMs is larger than

the information depth for Al in such a sample. This implies two things: 1) detected Al fluorescence is produced mainly in the feldspar grains of the top layer. 2) the Al in many of the feldspar grains does not suffer the absorption effect of the Fe in the adjacent olivine grains. When the samples are ground to particle sizes smaller than the information depth of Al in the nanopowder, part of the produced Al fluorescence can be detected even though it underwent absorption by olivine nanograins. This also explains why the Mg does not suffer in the same way despite also being a light element. The Mg is abundant in the Fe-rich olivine and therefore even in the original sample suffered the absorption effects of Fe.

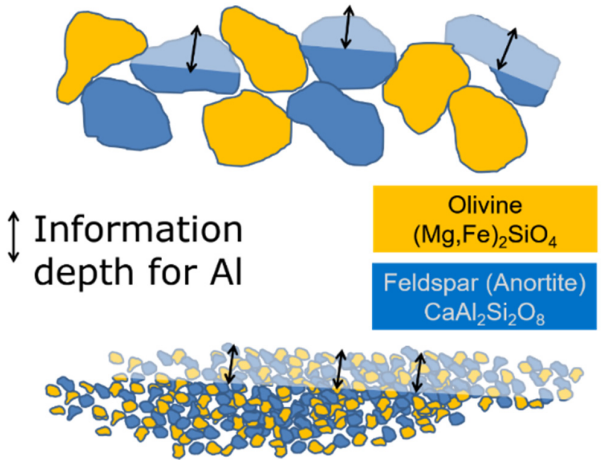

Figure 10. Schematic explanation of matrix effects on powder samples in relation to information depth. After grinding the grains of the sample smaller than the information depth limit, the samples would not give a representative spectrum for its bulk composition and should not be used for calibration.

This effect is not only relevant for µ-XRF, but for all XRF techniques that do not undergo an extensive sample preparation or dilution. Nanopowders can fulfil the requirement of homogeneity and infinite thickness as their homogeneity is comparable to what is found in glass samples. If standard powder samples (usually 63 - 150 µm grain size) are used as reference materials, it must be considered that secondary effects are not well represented by the sample therefore the matrix "correction" expected from a reference sample is wrong and would surely provide wrong results on a homogenous sample suitable for quantitative analysis.

As previously discussed, an FP-quantification would, in principle, perform the correct matrix correction and obtain "correct" concentrations on the unknown sample. On the other hand, it would fail on the reference sample because this cannot be considered as homogenous – a prerequisite for bulk quantification. Reference samples are often given more credit than they might deserve. Especially for microbeam analysis the accuracy of a pure FP quantification nowadays already might surpass the uncertainties of the used standards.

Not all elements suffer such strong matrix effects. These effects are mainly limited to major elements and is more likely present in the interaction of light elements with heavy components in samples, e.g., Al in Fe. If we consider trace elements, particularly in combination with high

energy lines, these effects (e.g., K-lines from Rb, Sr, Y, Zr, and Nb) can become negligible. This can be shown for geological samples. In geological processes these elements tend to fractionate, possibly during the mineral/rock formation or during weathering. This fractionation and the high sensitivity of XRF are two factors that make these elements also ideal for ceramic and obsidian provenance studies (e.g., [17]).

To illustrate the quantification of trace elements in minerals, a garnet thick-section was analysed. The sample comes from the Zillertal locality in Australia. For the calibration, the 9 nanosamples were used. To remove diffraction peaks and improve the peak to background in the high energy range, the garnet was measured using a strong filter primary filter composed of 100 µm Al, 50 µm Ti, and 25 µm Cu. The reference samples used were: GH, BHVO-2, JA-2, SARM-1, JR-2, AC-E, RMG-1, JA-2, JB-2, and NIST 620 for trace element values [GeoREM 18].

To illustrate the quantification of trace elements from the most "pristine" data evaluation point, net intensities were used (Fig. 11). These were determined for the element in question by deconvolution. Net intensities were plotted against the measured concentration in the sample. The slope was calculated and forced through 0. The slope represents the sensitivity of the instrument for the given measurement conditions and sample type e.g., a rock or mineral. For example, for Rb the slope is 0.6969, which represents 0.6969 counts per second per ppm of Rb in the sample. From this it is possible to infer not only the composition, but also the required measurement time needed to achieve a certain precision if the counting statistic error is the square root of the intensity.

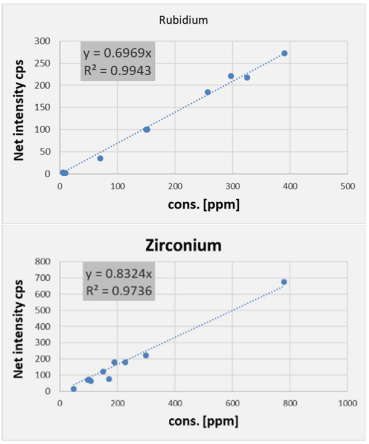

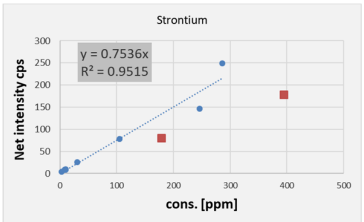

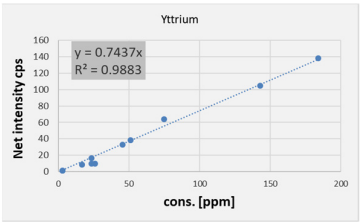

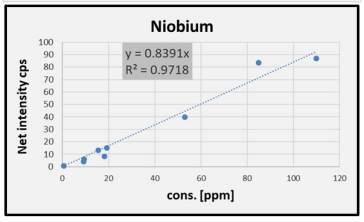

Z	Element	count/s/ppm	count/s/ppm
37	Rb	0.6969	
38	Sr	0.5889	0.7536
39	Y	0.7438	
40	Zr	0.8279	
41	Nb	0.8391	

Figure 11. Correlation of the net peak intensity with the composition of the samples. Note for 4 of the 5 elements the correlations are almost perfect. Some of the reference values for Sr seem to be incorrect using the adjacent elements it is possible to infer that the two red squares are probably not good and the new sensitivity value for Sr is 0.7536 counts/s/ppm.

For such a sample system, it is expected that all the points fall in a line. This is the case for most of the elements except for Sr. In the compilation of GEOREM database [18), there are several values compiled for the Sr reference samples, and therefore there is already an uncertainty. The low number of points makes it difficult to determine what reference sample should be excluded. However, the complete group of elements from Rb to Nb should behave consistently, either showing an increasing or decreasing of their instrument sensitivity, depending on instrument parameters. Their lines are very close to each other's, thus we can use them to interpolate the sensitivity of the element in between. By plotting the sensitivities, it is possible to recognise that the Sr sensitivity does not fit. Knowing the expected sensitivity, we can re-evaluate the validity of the calibration points and recognize the outliers. By eliminating two samples, the complete group of elements and Sr become consistent.

Using this sensitivity, it is possible to quantify the different regions of the garnet. As can be seen in the element distribution image (Fig. 12), the garnet shows a strong zonation with and enrichment in Mn and Y in the centre. Quantitative analysis results from different regions of the garnet are given in the table below.

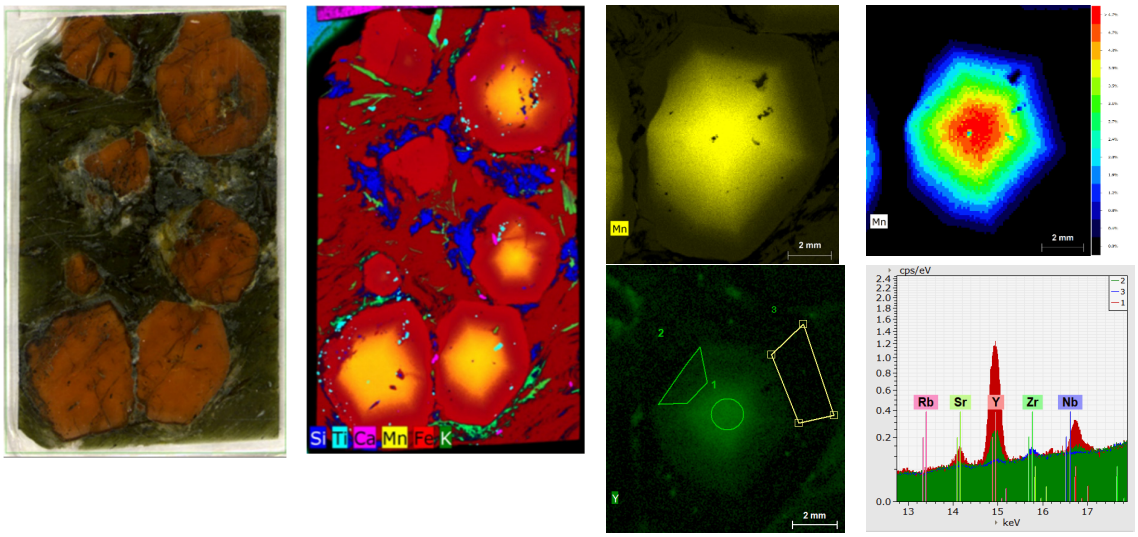

Figure 12. The fist picture shows a think section of a garnet sample, and the second an elemental distribution map. For the bottom left crystal an additional scan was performed using a primary filter. From this measurement the Mn distribution as intensity and as quantify map. Additionally, the distribution of the element Y is displayed. From this map, tree regions of interest were selected (1 in the centre of the grain, 2 toward the edge and 3 outer rim. The spectra of these regions are shown to the right. By using the previous calibration and the net peak intensity is possible to quantify the different region of the map. The Y concertation found in the garnet changes from 400 ppm in the centre to 60 ppm in the region 2 and down to 3 ppm on the rim.

With μ-XRF it is possible study complex non-homogeneous samples and obtain information of chemical variations from the major to the trace element level. As stated in ASTM E2926-13, something that should always be considered when working with analytical equipment and complex samples and tasks (including quantification using FP or reference samples), no algorithms can fully replace knowledge, skills, ability, experience, education or training and should be used in conjunction with professional judgment.

4.2. What else can be done with μ-XRF?

Many of the features of μ-XRF as an analytical technique can be illustrated best by using examples. The following pages summarise some of these features and provide a brief explanation of the physics behind the process. The examples are short and the list does not intend to cover all the possibilities or even discuss all relevant parameters and limitations. The topics mainly cover how μ-XRF can be used to obtain more information from a sample when considering such things as: composition and compositional variation, crystallinity, and 3D structure.

4.2.1. Diffractoscopy, or Laue mapping. In μ-XRF, diffraction peaks are considered to be the most prominent measurement artefact, and they complicate the elemental compositional analysis. They originate from constructive interference of scattered X-rays in a crystalline sample. According to Bragg's law, they occur when the crystal lattice and orientation match incident angle and wavelength of the incident X-rays. With the focussed X-ray beam and the large solid angle of detection a large range of possible angles is available. The X-ray beam is "white light" as it has all wavelengths between 1 nm and 0.01 nm. Thus, it is very likely to detect a diffraction feature anywhere in the spectrum when a crystalline sample is measured. As in the case of the steels and minerals, primary X-ray beam filters can be used to eliminate them. Despite their complications, diffraction peaks contain important information, i.e., they are a signature of the crystalline structure of the sample. The examples in Fig. 13 show Laue maps of a single Si crystal, a twin NdGaO3 crystal, and multi-crystalline silicon wafer.

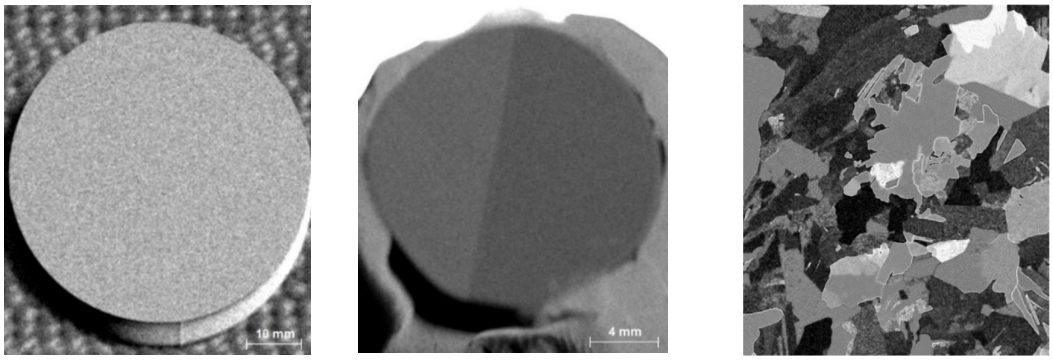

Figure 13. Image at left shows the intensity distribution of Bragg peaks on a silicon single crystal, the middle image is the distribution on a NdGaO3 twin crystal, and on the right, a multi-crystalline Si wafer.

In X-ray maps, element distribution is created by the elemental signal. In Laue maps, the contrast in the images is given by the intensity variation of the different diffraction peak. Using diffraction information this way does not yield any insight into crystal orientation, but it can produce a wealth of information about the size and position of individual crystal domains, which can be useful in many fields (Fig. 14).

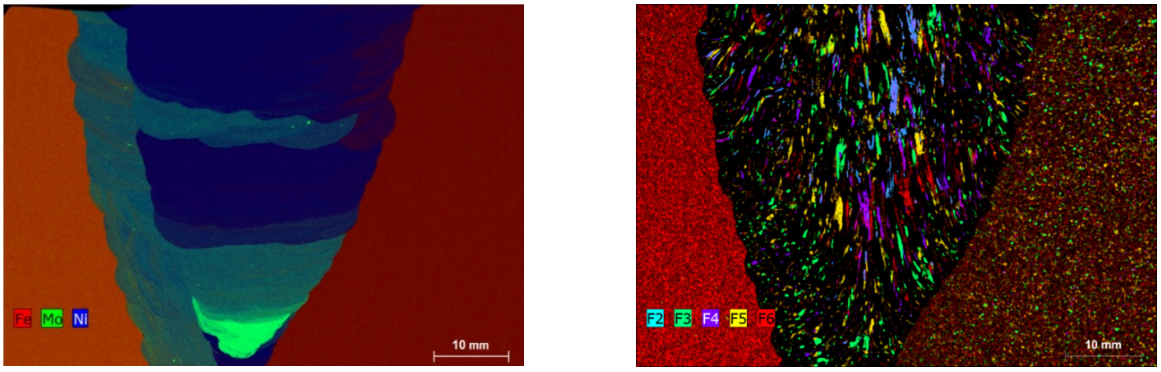

Figure 14. A prepared and polished welding joint was mapped. The map on the left is an elemental distribution map. At right, a Laue map. In the Laue map, right side and left side of the sample are two different types of steel, in the middle is the welding material. The elemental distribution map at left was obtained using a strong primary filter and here the composition of the samples can be studied in detail. The Laue map at right was acquired without filters. Here it is possible to visualise and map the diffraction features. The size of the domains relates to the size of the crystallites within the sample, so the crystal domain in the central part of the welding joint with large inner crystals and smaller crystals at the edges show that the cooling process is much faster near the edge.

A benefit of this approach is that samples can be scanned to determine the location of crystal domains. These locations can be later measured with diffractometers to determine crystal parameters.

4.3. Looking into the depths of matter

The spatial resolution of μ-XRF is, especially when compared to SEM-EDX, much coarser in all three dimensions, and it is extremely difficult to improve this. Sample information depth allows us to "see", not only micrometres, but possibly even millimetres into the sample. The penetration depth of X-rays (resolution) is a physical property, which cannot be changed efficiently. On the other hand, μ-XRF may open the 3rd dimension for compositional studies. In this section some possibilities how to analyse complex 3D samples are shown.

4.3.1. Layer analysis. One common way to utilize the penetrating character of X-rays is measuring the thickness of layered structures. While travelling through matter the radiation is attenuated, but also produces fluorescence on its path into the sample. This fluorescence

intensity is then a measure for the thickness of the layer(s). Technically, it is the number of atoms in the beam path that are measured, and not thickness directly. This means that the density of the layered material is the most crucial parameter when converting the mass deposition (i.e., number of atoms per unit area) into the layer thickness. Unfortunately, density is not a well-known parameter, particularly for very thin layers and heavily depending on the layer deposition method. Nevertheless, it is more straightforward to consider thickness when addressing some general guidelines for this type of application.

The applicability of X-ray layer thickness determination depends greatly on the sample system. For some layer structures the penetration depth may be the restricting parameter (for instance, Sn-rich solder layers), other samples are limited by the information depth of the produced fluorescence (most light-element layers). The measurement geometry also plays a large role. If both excitation and fluorescence radiation are detected (quasi-)perpendicular, maximum measurable layer thicknesses are achieved. With lower angles the virtual layer thickness becomes larger, and hence the thickness range is more limited. On the other hand, very thin layers might be measured more precisely under shallow angles, as they are effectively thicker and produce more fluorescence signal.

Theoretically, the number of layers in a multi-layer system that can be analysed can be very large. In practice, the restriction is the abundance of an element in multiple layers (it is difficult to differentiate how much signal comes from which layer) or light element layers (when covered by another layer their fluorescence might not be detectable anymore). In addition, the number of elements per layer is – theoretically – unlimited. Again, the main problem will be repeated elements, and with more elements per layer a repetition becomes more likely.

In general, it can be said that metal layer stacks (where K-lines are used) of up to 30 µm thickness can be measured for their thickness and composition. On the other hand, for a heavy matrix such as a layer of Au, where the L-lines are used for measurement, the layer becomes infinitely thick above ~ 5 µm. For light element layers, often the thickness can best be determined by not using the layer's fluorescence intensity but by considering their absorption effect on the base material fluorescence. Micro-XRF is a standard analytical tool in industrial layer analysis because it is possible to determine noninvasively and with high precision not only the thickness of the layers in a sample but also the composition of the layer if it is not made from a single element. The quantification can be done based on fundamental parameters or on standards or a combination of them with reference samples. For calculation, some information requires including the layer sequence as well as the density of the layers in question.

4.3.2. Dealing with a divergent beam. Mapping a sample with 5 mm topography and using an aperture keeps the beam diameter over the sample below 50 µm as the divergence of the beam is reduced significantly (Fig. 15). The effect can be seen in Fig. 16, were the Cr-zonation bands on the emerald can be measured with a narrow beam using and 500 µm aperture for a larger sample depth.

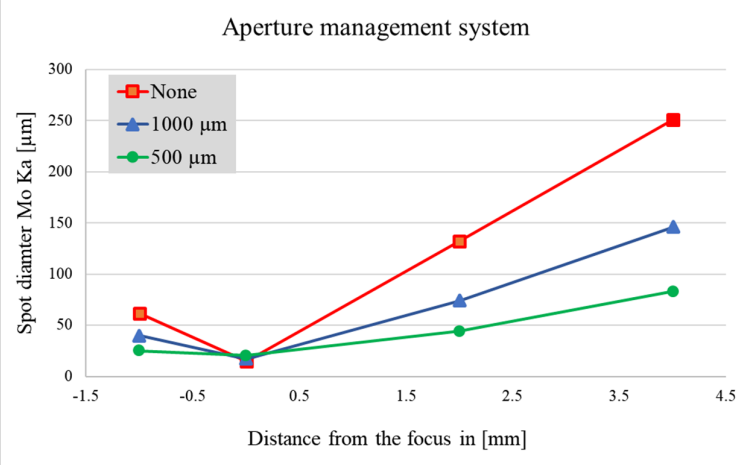

Figure 15. The diagram shows the effect of the AMS on beam divergence. Insert a 500 µm aperture in the path and the beam diameter remains below 100 µm even 4 mm from the focal point.

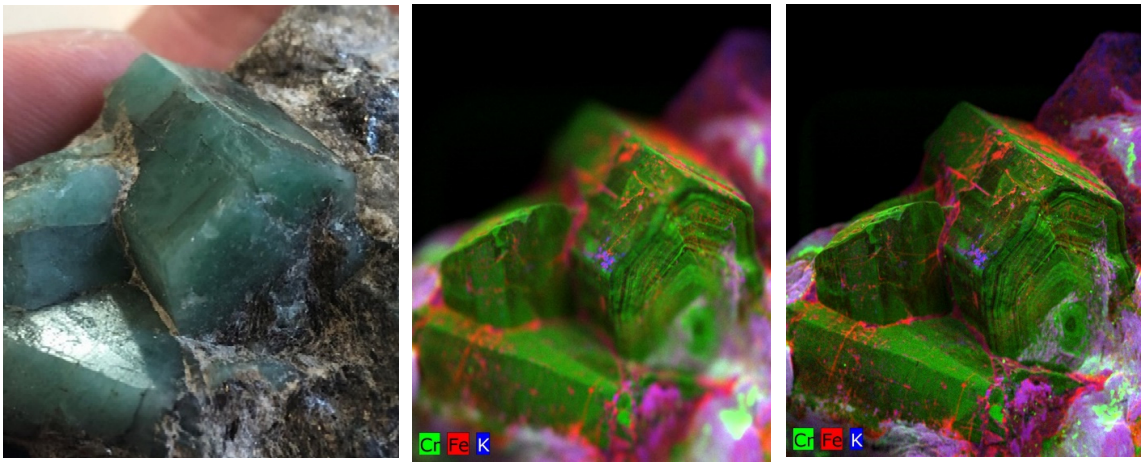

Figure 16. The effect of the beam divergence is shown on an emerald. The width of the central crystal is ~1 cm, left picture. The first element distribution (middle map) was collected without the AMS and the focal depth is few millimetres below the top of the sample (sharp plane). Below and above this plane the image becomes blurry due to beam divergence. In the image at, right the focal depth has increased and a better spatial resolution is achieved.

The reduction of the beam divergence is associated with a loss of intensity this, however, can be overcome by increasing the current or the measurement time. When an AMS is used and the beam divergence is reduced, it not only influences the focal depth, but it also influences the width of diffractions peaks, improving the performance when the instrument is used to study diffraction features on a sample.

4.3.3. Visualising scattering

In Fig. 17, the elemental distribution of tektite is shown. Tektites are natural glasses, which are produced during a major impact of a meteorite to the Earth [20]. The tektite shown here was

found in Cambodia and is related to the Australasian tektite strewn field. The molten glass is known to be extremely poor in water, but abundant gas bubbles can be found inside the glass tektites. The tektite (Fig. 17) was cut and polished for measurement. The Fe elemental distribution at left shows the mingling of different glass components shown by the differences in intensity, as well as some gas bubbles (holes) that are disrupting the schlieren (giving a time constraint for the formation of the bubbles). The bubbles in the centre part of the sample are more deformed than those in the outer rim of the tektite. This is likely related to different cooling speeds. The image at right is a map of the high energy scattering between 18 keV and 35 keV. In this range no element signal is recoded but includes the Compton, Rayleigh, and bremsstrahlung scattering. The scattering is proportional to the average atomic number of the sample in the given volume and is observed as grayscale differences. The information depth (see Fig. 3) can be estimated between 1 mm and 3 mm. In this case, we can detect directly some still hidden gas bubbles below the material surface.

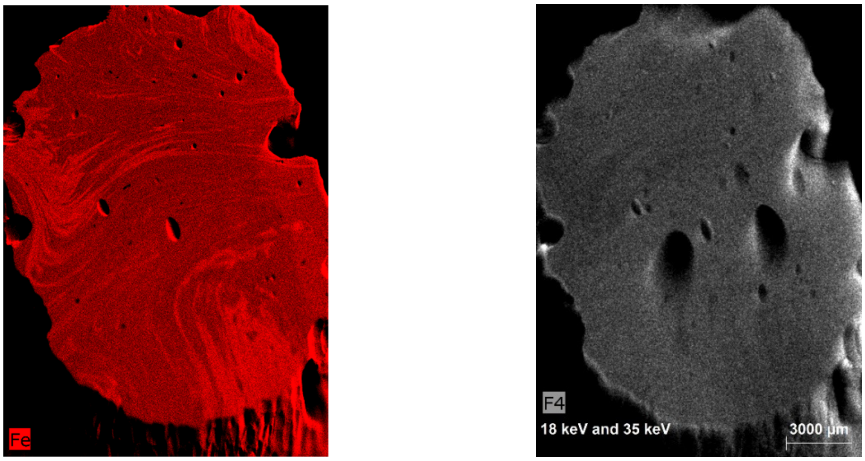

Figure 17. µ-XRF scan on a tektite, left image shows the Fe element map. Right image- the scattering in the range between 18 and 35 keV, a range including Compton, Rayleigh as well as bremsstrahlung scattering.

4.3.4. Going 3D - Confocal µ-XRF. The application shown above, especially the layer analysis and the in-depth density contrast maps, make use of the penetration depth of high energy X-rays. In both cases the signal from depth is overlaid with the signal from the surface and needs to be separated. Ideally, information from defined depths could be obtained without interference from another signal. In order to achieve this, the field of view of the detector can be restricted to a very small cross section by use of a second polycapillary optics. This optics, just like the focussing optics in the excitation beam, has a focal spot. If this is aligned with the focal spot of the excitation beam the detector only 'sees' fluorescence produced in a probing volume, which dimensions are defined by the focal spot sizes of both lenses and the geometry of the measurement system. The smallest probing volume is achieved when excitation beam and detection beam path intersect at an angle of 90°.

This method is ideally used for detecting medium- or high-Z elements in a low-Z matrix for two reasons: 1) With this setup, depth resolutions on the order of 20 µm can be attained. To effectively apply the Z-resolution of the system the information depths of the probed elements should be an order of magnitude higher. 2) the transmission properties of the second optic, much more than that of the first, restrict the elements which can be efficiently probed. The energy range with significant transmission ranges from about 4 keV to 15 keV.

Some application examples are from the field or art and conservation (e.g., [8]) or technology including the distribution of additives in polymers, accumulation of elements in organic matter, or metallic contaminants in aluminium sheet/foil production (Fig. 18).

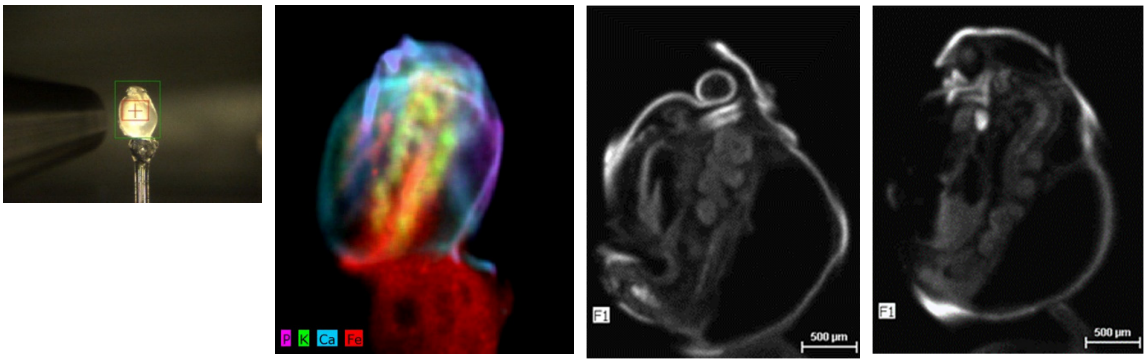

Figure 18. Measurement was performed for a specially prepared water flea. The sample is ~ 3 mm high. The first image is an image of the sample. The second shows element distribution and the last two depict the total intensity at two different depths measured with a confocal approach; here the total intensity is displayed. Note the differing details in the images.

4.3.5. Preparative 3D µ-XRF. As discussed above, large information depths for the elements of interest in the sample enable minimally invasive X-ray analysis with, for example, a confocal setup. However, if the volume of interest is larger than what the information depth of the µ-XRF allows either because of a heavy matrix or because light elements are essential, a more invasive approach is required. Utilising computed tomography (CT), it is possible to obtain non-invasive 3D information of large samples. The primary information collected is basically a density or average atomic number contrast, but no information on the chemical element distribution is collected. This, then, requires direct access to multiple levels of information depth, such as in the approached describe below. This approach is fully invasive as sample volume is polished away by layers for µ-XRF chemical reconstruction. The sample selected for the study is an iron meteorite. The Gujba meteorite is composed of millimetre size metal nodules of variable composition, as well as a significant silicate fraction. Its formation is still a controversial topic. The project described below consists of a set of 36 scans performed after removing 150 µm layers of sample, totalling 5.18 mm of sample (Fig. 19). The multiple element maps acquired were superimposed for reconstruction using a 3D software. The information obtained allowed visualisation of the compositional variation of a complex sample to an extremely high level.

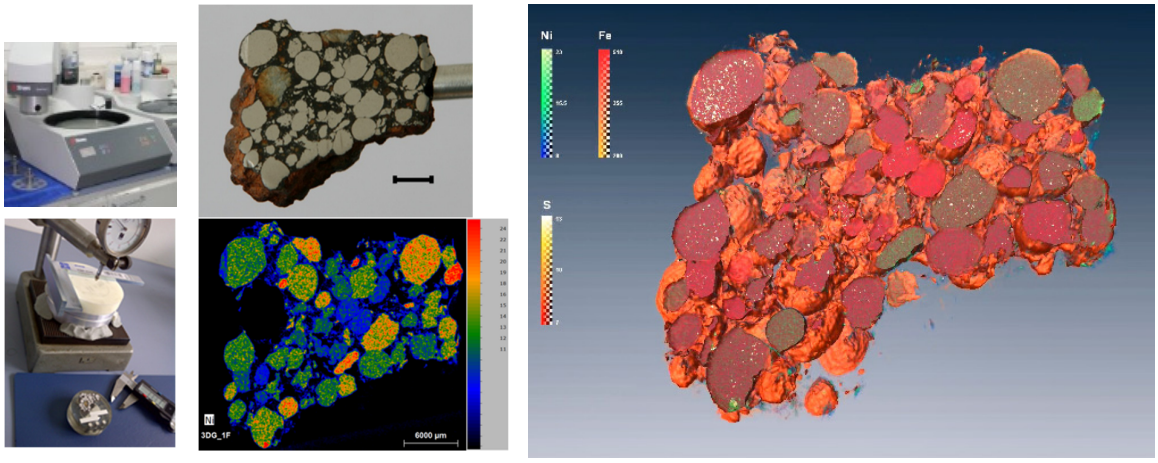

Figure 19. Invasive and destructive 3D µ-XRF. A total of 36 150 µm thick layers were exposed and then measured. The 36 layers were reconstructed using a 3D software. From top-left to right: polishing machine, measurement tool for ensuring sample removal, full sample, map from a single layer and reconstructed 3D image from Ni, Fe and S maps.

Despite being a time-consuming and destructive approach, this is thus far the only analytical procedure allowing study of such large sample volumes with high spatial resolution and compositional information. The data blocked obtain from the measurement contains the digitalized compositional variation of the sample for all elements detectable under the given measurement conditions.

5. OUTLOOK

The data and results presented here are intended to illustrate just some of the possibilities of µ-XRF not only as a pre-screening technique but also as a versatile analytical tool. The acceptance of this technique has increased in recent years due to its broad range of application and the required minimal sample preparation. The wider distribution is illustrated in the increasing number of academic publications. However, despite being a mature technique, a variety of developments are still taking place. Not only to apply it on an even wider variety of samples but also using it in completely new fields of application, such as automated mineral analysis. Further work is also done to take fundamental parameter quantification to the next level. The current and future improvements will most likely help this niche technique to become a standard for material analysis.

6. REFERENCES

[1] Jaklevic M M, French W R, Clarkson T W and Greenwood M R 1978 X-ray fluorescence analysis applied to small samples. *Adv. X-ray Anal.* **21** 171-185

[2] Toribara T Y, Jackson D A, French W R, Thompson A C and Jaklevic J M 1982 Nondestructive X-ray fluorescence spectrometry for determination of trace elements along a single strand of hair. *Anal. Chem.* **54** 1844-1849

[3] Nichols M C, Boehme D R, Ryon R W, Wherry D, Cross B and Aden G 1987 Parameters affecting X-ray microfluorescence (XRMF) analysis. *Adv. X-ray Anal.* **30** 45-51

[4] Cross B J and Wherry D C 1988 X-ray microfluorescence analyzer for multilayer metal films. *Thin Solid Films* **166** 263-272
Boehme D R 1987 X-ray microfluorescence of geologic materials. *Adv. X-ray Anal.* **30** 39-44

[5] Carpenter D A, Taylor M A and Holcombe C E 1989 Applications of laboratory X-ray microprobe to materials analysis. *Adv. X-ray Anal.* **32** 115-120

[6] Carpenter D A and Taylor M A 1991 Fast, high-resolution X-ray microfluorescence imaging. *Adv. X-ray Anal.* **34** 217-221
Nicolosi J A, Scruggs B and Haschke M 1998 Analysis of sub-mm structures in large bulky samples using micro-X-ray fluorescent spectrometry. *Adv. X-ray Anal.* **41**

[7] Edax Product Profile 1997 Spectral mapping.
M. ImatZu 1997 Development of fast texture mapping system with energy-dispersive X-ray diffraction method. *Adv. X-ray Anal.* **40**

[8] Lachmann T, Van der Snickt G, Haschke M and Mantouvalou I 1989 Combined 1D, 2D and 3D micro-XRF techniques for the analysis of illuminated manuscripts. *J. Anal. Atom. Spectrom.* **31**

[9] Wolff T 2009 *Referenzprobenfreie quantitative Mikro-Röntgenfluoreszenzanalyse*. PhD-thesis. (Berlin, Germany: Technische Universität Berlin) http://dx.doi.org/10.14279/depositonce-2299

[10] Beckhoff B, Kanngiesser B, Langhoff N, Wedell R and Wolff H (Eds.) 2006 *Handbook of practical X-ray fluorescence analysis*. (Berlin, Germany: Springer).

[11] Plusquellec G, Geiker M R, Lindgard J and De Weerdt K 2018 Determining the free alkali metal content in concrete – Case study of an ASR-affected dam. *Cement Concrete Res.* **105** 111-125

[12] Sherman J 1955 The theoretical derivation of fluorescent X-ray intensities from mixtures. *Spectrochim. Acta* **7** 283-30.

[13] Scofield J H 1974 *Phys. Rev. A* **9** 1041

[14] Salem S I, Panossian S L and Krause R A 1974 *Atom. Data Nucl. Data* **14** 91

[15] Ertuğral B, Apaydın G, Çevik U, Ertuğrul M and Kobya A 2007 *Radiat. Phys. Chem.* **76** 15

[16] Elam W T, Ravel B D and Sieber J R 2002 *Radiat. Phys. Chem.* **63** 121

[17] Nazaroff A J, Prufer K M and Drake B L 2010 Assessing the applicability of portable X-ray fluorescence spectrometry for obsidian provenance research in the Maya lowlands. *J. Archaeol. Sci.* **37** 885-895

[18] Jochum K P, Nohl U, Herwig K, Lammel E, Stoll B and Hofmann A W 2005 GeoReM: A new geochemical database for reference materials and isotopic standards. *Geostand. Geoanal. Res.* **29** 333-338

[19] Röhrs S and Stege H 2004 Analysing Limoges painted enamels from the 16th to 19th centuries by using a portable micro X-ray fluorescence spectrometer. *X-ray Spectrom.* **33** 396-401

[20] Goderis S, Tagle R, Fritz J, Bartoschewitz R and Artemieva N 2017 On the nature of the Ni-rich component in splash-form Australasian tektites. *Geochim. Cosmochimica Acta* **217** 28-50

[21] Wolff T 2018 Full spectrum modeling: Understanding the matter. in: Denver X-ray Conference. (Westminster, CO)